Acta Crystallographica Section B
Structural Science
ISSN 0108-7681

Hidden superlattice in $Tl_2(SC_6H_4S)$ and $Tl_2(SeC_6H_4Se)$ solved from powder X-ray diffraction

Kevin H. Stone,[a]‡ Dayna L. Turner,[b]§ Mayank Pratap Singh,[b] Thomas P. Vaid[b]* and Peter W. Stephens[a]*

[a]Department of Physics and Astronomy, Stony Brook University, Stony Brook, NY 11794-3800, USA, and [b]Department of Chemistry, The University of Alabama, Tuscaloosa, Alabama 35487, USA

‡ Present address: Materials Science Division, Lawrence Berkeley Lab, Berkeley, CA 94720, USA.
§ Present address: Novus International, 20 Research Park Drive, St Charles, MO 63304, USA.

Correspondence e-mail: tpvaid@ua.edu, pstephens@stonybrook.edu

Received 3 May 2011
Accepted 30 July 2011

The crystal structures of the isostructural title compounds poly[(μ-benzene-1,4-dithiolato)dithallium], $Tl_2(SC_6H_4S)$, and poly[(μ-benzene-1,4-diselenolato)dithallium], $Tl_2(SeC_6H_4Se)$, were solved by simulated annealing from high-resolution synchrotron X-ray powder diffraction. Rietveld refinements of an initial structure with one formula unit per triclinic cell gave satisfactory agreement with the data, but led to a structure with impossibly close non-bonded contacts. A disordered model was proposed to alleviate this problem, but an alternative supercell structure leads to slightly improved agreement with the data. The isostructural superlattice structures were confirmed for both compounds through additional data collection, with substantially better counting statistics, which revealed the presence of very weak superlattice peaks not previously seen. Overall, each structure contains Tl—S or Tl—Se two-dimensional networks, connected by phenylene bridges. The sulfur (or selenium) coordination sphere around each thallium is a highly distorted square pyramid or a 'see-saw' shape, depending upon how many Tl—S or Tl—Se interactions are considered to be bonds. In addition, the two compounds contain pairs of Tl^I ions that interact through a closed-shell 'thallophilic' interaction: in the sulfur compound there are two inequivalent pairs of Tl atoms with Tl—Tl distances of 3.49 and 3.58 Å, while in the selenium compound those Tl—Tl interactions are at 3.54 and 3.63 Å.

1. Introduction

The isostructural compounds $Tl_2(SC_6H_4S)$ and $Tl_2(SeC_6H_4Se)$ were synthesized as part of a study on the possible electrical conductivity of metal-arenethiolate and metal-areneselenolate network solids (Turner *et al.*, 2008, 2010). These two compounds each contain two-dimensional networks of Tl and S or Tl and Se, yet neither has significant electrical conductivity. Both contain pairs of Tl ions with closed-shell $Tl^I\cdots Tl^I$ interactions, as described below.

Both compounds were initially indexed as triclinic with volumes of roughly 200 $Å^3$, but ultimately determined to possess a $2^{1/2} \times 2^{1/2}$ $R45^\circ$ superlattice structure. Typically, superlattices are recognized by the presence of superlattice peaks, which may be weak and/or broad compared with the rest of the Bragg peaks in a diffraction pattern. Here we present a case where a superlattice was determined primarily through the constraints imposed by the requirement of physically acceptable interatomic distances, as well as through a subtle, but significant, improvement in the fit to the data.

Several Tl^I thiolates have been reported and they exhibit a remarkable diversity in their structures. The *tert*-butyl thiolate crystallizes as an octomeric molecule, $Tl_8(S^tBu)_8$ (Krebs & Brömmelhaus, 1989, 1991). Thallium(I) thiophenolate, in

Table 1
Experimental details.

For all structures: triclinic, $P\bar{1}$, $Z = 4$. Experiments were carried out at 298 K using a Huber diffractometer. Refinement was with 0 restraints. H-atom parameters were not refined.

	$Tl_2SC_6H_4S$	$Tl_2SeC_6H_4Se$
Crystal data		
Chemical formula	$Tl_2(SC_6H_2S)$	$Tl_2(SeC_6H_2Se)$
M_r	549.0	642.8
a, b, c (Å)	6.5525 (3), 6.8444 (3), 9.5265 (2)	6.67438 (8), 6.84998 (8), 9.82649 (10)
α, β, γ (°)	71.798 (2), 85.988 (2), 89.219 (2)	72.513 (2), 84.790 (2), 88.659 (3)
V (Å^3)	404.85 (9)	426.72 (1)
Radiation type	Synchrotron, $\lambda = 0.698163$ Å	Synchrotron, $\lambda = 0.699855$ Å
μ (mm^{-1})	37	43
Specimen shape, size (mm)	Cylinder, 8 × 0.7	Flat sheet, 8 × 17
Data collection		
Specimen mounting	Sample was mounted in a thin-walled glass capillary of nominal diameter 0.7 mm	Flat-plate geometry on zero-background holder
Data collection mode	Transmission	Reflection
Scan method	Step	Step
2θ values (°)	$2\theta_{min} = 2$, $2\theta_{max} = 30$, $2\theta_{step} = 0.005$	$2\theta_{min} = 3$, $2\theta_{max} = 40$, $2\theta_{step} = 0.005$
Refinement		
R factors and goodness-of-fit	$R_p = 0.070$, $R_{wp} = 0.080$, $R_{exp} = 0.065$, $R_{Bragg} = 0.019$, $\chi^2 = 1.484$	$R_p = 0.049$, $R_{wp} = 0.056$, $R_{exp} = 0.020$, $R_{Bragg} = 0.026$, $\chi^2 = 7.756$
No. of data points	5601	7401
No. of parameters	57	94

Computer programs used: spec, *TOPAS-Academic* (Coelho, 2007), X16C beamline software, *ORTEP*-3 for Windows (Farrugia, 1997), *Mercury* (Version 2.2; Macrae *et al.*, 2006) and *publCIF* (Westrip, 2010).

contrast, forms ionic clusters that are linked by bridging Tl ions in the solid state and can be formulated as $[Tl_5(SPh)_6]^-[Tl_7(SPh)_6]^+$ (Krebs & Brömmelhaus, 1989, 1991). The benzyl thiolate forms extended edge-sharing Tl_2S_2 squares in a kinked-ladder arrangement, as does thallium(I) 2,4,6-tris(trifluoromethyl)thiophenolate (Labahn *et al.*, 1991). The structure of thallium(I) *n*-propylthiolate can be viewed as $Tl_4(SC_3H_7)_5^-$ clusters linked by Tl^+ cations to form infinite chains in the solid state (Hammerschmidt *et al.*, 2005). Finally, the reported compound most closely related to $Tl_2(SC_6H_4S)$ is $[NEt_4]_2[Tl_2(S_2C_6H_4)_2]$ (Bosch *et al.*, 1996), where $S_2C_6H_4$ is 1,2-benzenedithiolate, in contrast to the 1,4-benzenedithiolate of $Tl_2(SC_6H_4S)$. In the $Tl_2(S_2C_6H_4)_2^{2-}$ anion each Tl^I is bonded to the four S atoms of the $S_2C_6H_4$ ligands and the two Tl^I ions are separated by 3.5116 (4) Å, indicating a closed-shell $Tl^I\cdots Tl^I$ 'thallophilic' bonding interaction.

2. Experimental

Reactions were carried out under N_2 in degassed ethylenediamine; the products are mildly air-sensitive and were protected from air after benchtop workup. Reagents were purchased from commercial suppliers and used as received. The reagent 1,4-benzenedithiol was prepared from 1,4-bis(isopropylthio)benzene (Testaferri *et al.*, 1983), which was reduced by sodium in liquid ammonia to yield 1,4-benzenedithiol (Adams & Ferretti, 1959). The protected selenol 1,4-di(acetylseleno)benzene was prepared according to literature procedures (de Boer *et al.*, 2003). IR spectra were obtained on a Perkin–Elmer Spectrum BX FT-IR system as Nujol mulls on NaCl plates. Microanalysis was performed by the University of Illinois Microanalysis Laboratory. In both syntheses the resulting samples consisted of crystallites too small to be used for single-crystal analysis, but powders were of sufficient quality for high-resolution X-ray diffraction studies.

$Tl_2(SC_6H_4S)$: Thallium acetate (0.185 g, 0.703 mmol) and 1,4-benzenedithiol (0.050 g, 0.352 mmol) were combined in 8 ml of ethylenediamine. The suspension was heated to reflux for 16 h and then cooled to room temperature. The yellow precipitate was isolated by filtration and washed with methanol and ether. Yield of yellow $Tl_2(SC_6H_4S)$: 0.155 g, 80%. IR (Nujol, cm^{-1}): 1245 (w), 1131 (w), 1096 (s), 1002 (m), 819 (m) (665) w). Anal.: calc. for $C_6H_4S_2Tl_2$: C 13.13, H 0.73, N 0.00; found: C 13.56, H 0.63, N 0.00.

$Tl_2(SeC_6H_4Se)$: Thallium acetate (0.131 g, 0.499 mmol) and 1,4-(diacetylseleno)benzene (0.080 g, 0.249 mmol) were separately dissolved in ethylenediamine. The TlOAc solution was added to the ligand solution, whereupon a red precipitate formed immediately. The suspension was heated to reflux for 16 h then cooled to room temperature. The red precipitate was isolated by filtration and washed with methanol and ether. Yield of $Tl_2(SeC_6H_4Se)$: 0.142 g, 88%. IR (Nujol, cm^{-1}): 1104 (w), 1070 (s), 999 (s), 812 (s), 666 (w). Anal.: calc. for $C_6H_4Se_2Tl_2$: C 11.21, H 0.63, N 0.00; found: C 11.56, H 0.58, N 0.0.

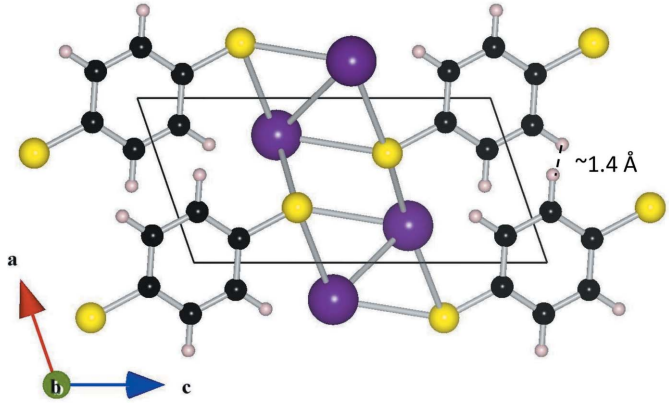

Figure 1
Initial structure of $Tl_2(SC_6H_4S)$ viewed along the *b* axis. The Se compound is essentially identical. The C_6H_4 units lie almost in the *ac* plane and the implausible 1.4 Å H—H distance is indicated.

Table 2
Lattice dimensions and refinement statistics for the various models discussed.

In both cases superlattice (2) is the final refined structure.

	$Tl_2(SC_6H_4S)$			$Tl_2(SeC_6H_4Se)$		
Lattice	Disordered	Superlattice (1)	Superlattice (2)	Disordered	Superlattice (1)	Superlattice (2)
a (Å)	4.7054 (3)	6.5525 (4)	6.5525 (4)	4.7256 (3)	6.6744 (4)	6.6744 (4)
b (Å)	4.7698 (3)	6.8444 (4)	6.8444 (4)	4.8376 (3)	6.8500 (4)	6.8500 (4)
c (Å)	9.4219 (5)	9.4219 (5)	9.5265 (5)	9.6844 (5)	9. 6840 (5)	9.8265 (5)
α (°)	103.359 (2)	87.013 (2)	71.798 (2)	102.714 (2)	86.743 (2)	72.513 (2)
β (°)	99.116 (2)	73.623 (2)	85.987 (2)	98.219 (2)	74.886 (2)	84.790 (2)
γ (°)	92.495 (2)	89.218 (2)	89.218 (2)	91.488 (2)	88.659 (2)	88.659 (2)
R_{wp}	0.083	0.085	0.080	0.071	0.057	0.056
GOF	1.274	1.301	1.218	3.488	2.825	2.785

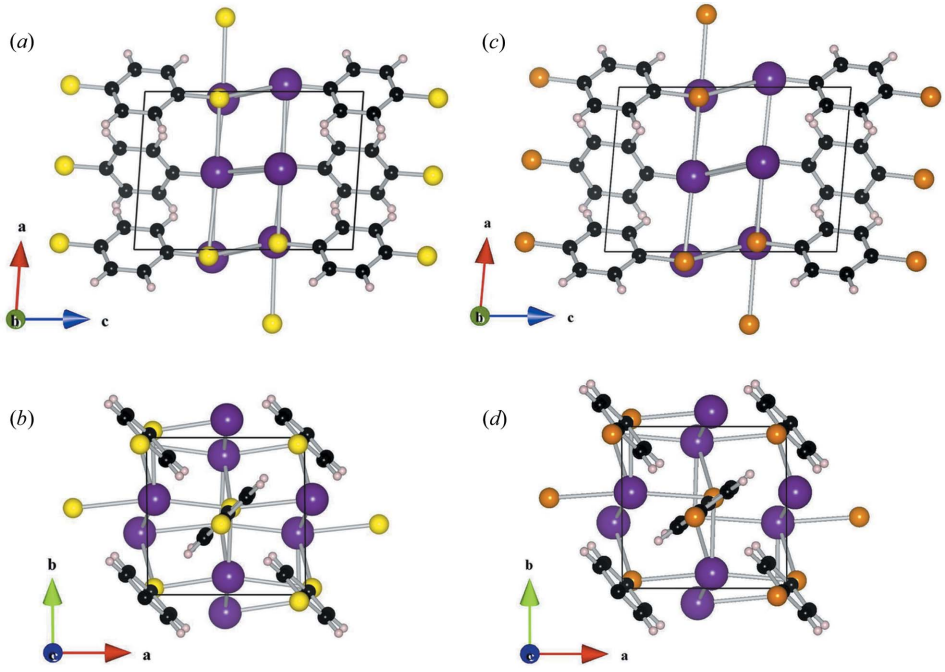

Figure 2
Structures of $Tl_2(SC_6H_4S)$ and $Tl_2(SeC_6H_4Se)$ viewed (*a*) and (*c*) along the *b* axis, and (*b*) and (*d*) along the *c* axis.

The X-ray data were collected over several different runs at NSLS beamline X16C with X-rays of ~ 0.7 Å wavelength. Samples were free-flowing powders which readily passed through a sieve with 50 µm holes, so no further grinding was warranted. The calculated X-ray absorption constant μ is rather large, of the order 400 mm^{-1}, and so it was necessary to collect powder data either in a flat plate or in a capillary with a diluted sample. Useful data from a capillary requires that its diameter should be no more than $\sim 2.5 \times \mu$, so it is advantageous to dilute the sample and use a larger capillary. Initial data were collected in standard Lindemann glass capillaries of 1 mm nominal diameter on samples diluted with finely ground cork. The degree of dilution was chosen empirically to maximize the signal. The S compound was solved and refined from that data set, but subsequently, in order to address the supercell issue discussed below, further data were collected over a limited range of angles. The sought-for superlattice peaks were not clearly visible in the original Se sample and so a second sample of higher crystallinity was subsequently prepared and measured in both flat plate and (diluted) capillary geometries. Once the possible superlattices were identified, additional scans in a flat plate were collected over narrow angular ranges. The flat-plate geometry afforded a much better signal-to-noise ratio, but suffered from a degree of preferred orientation, which was corrected using the March (1932)–Dollase (1986) model, constrained by a simultaneous fit to data from a (diluted) capillary sample. All data of each material were simultaneously refined to the same model. Samples were spun (capillaries) or rocked by 1° at each point (flat plate) during data collection. Indexing, structure solution by simulated annealing and refinement of the structural models were performed using *TOPAS-Academic* software (Coelho, 2003, 2007). Experimental details are given in Table 1.[1]

3. Crystal structure solutions

Initial diffraction patterns were readily indexed to triclinic lattices in which the *ab* lattice is nearly square: in $Tl_2(SC_6H_4S)$ a = 4.705, b = 4.770 Å, and γ = 92.5°, while in $Tl_2(SeC_6H_4Se)$ a = 4.725, b = 4.837 Å, and γ = 88.5°. Isostructural solutions were obtained in the space group $P\bar{1}$ with $Z = 1$ formula units in the unit cell, the aromatic ring centered on an inversion site and the Tl atom at a general position. This structure is illustrated in Fig. 1, and Rietveld refinements to the original data sets are shown in Fig. S1 of the supplementary material. The structure consists of a distorted square lattice of Tl atoms in the *ab*

[1] Supplementary data for this paper are available from the IUCr electronic archives (Reference: HW5016). Services for accessing these data are described at the back of the journal.

plane, separated by ~ 4.75 Å, with S or Se atoms at the center of the Tl squares. One side of this layer consists of the aromatic rings of the thiolate/selenolate ions; on the other side is another layer of Tl and S/Se atoms.

However, even though this structural model fits the powder X-ray data very well, it cannot be correct insofar as it contains very close intermolecular contacts between the aromatic rings, visible in Fig. 1. The high quality of the Rietveld refinements imply that the Tl and S/Se atoms have been located with reasonable accuracy, and so the solution must lie in the orientation of the aromatic rings. Tilting the rings by $\sim 45^\circ$ out of the *ac* plane would appear to solve the problem of close contacts, but this model gives a significantly worse fit and is not stable under refinement.

Our first attempts to solve the problem of neighboring rings being impossibly close was to introduce a disordered structure, with 50% occupancy of rings in the *ac* plane, and 50% occupancy perpendicular. Such a model gives a slightly improved fit and might allow the rings to stay out of each other's way, but a plausible description of the local order would be needed. Once an orientation is chosen for a given ring, its four neighbors in the *ab* plane must choose the opposite orientation, forcing long-range order within each *ab* plane into an alternating checkerboard pattern (as shown in Figs. 2*b* and *d*). This model could be rationalized by imagining that each *ab* layer has the checkerboard pattern, randomly stacked along *c*; however, the existence of a superlattice structure is also strongly suggested. This led us to consider the possibility of a $2^{1/2} \times 2^{1/2}$ *R*45° superlattice with in-plane translation vectors $\mathbf{a}_{\rm Super} = \mathbf{a}_{\rm Sub} + \mathbf{b}_{\rm Sub}$, $\mathbf{b}_{\rm Super} = \mathbf{a}_{\rm Sub} - \mathbf{b}_{\rm Sub}$. That leaves two possible choices for $\mathbf{c}_{\rm Super}$: $\mathbf{c}_{\rm Sub}$ or $\mathbf{c}_{\rm Sub} + \mathbf{a}_{\rm Sub}$, depending on the relative stacking of the 'checkerboards' of adjacent layers. Appropriately reduced, we denote these as supercell 1 and supercell 2. Refinement of the sulfur structures against the initial dataset shows a clear preference for supercell 2, followed by the disordered structure, supercell 1 and the worst fit being the original subcell structure. Close inspection of the original data, however, reveals no feature that might have been identified as a superlattice peak *a priori*. A similar trend was found for the selenium compound, in which both supercells gave comparable fits to the original data, followed by the disordered model, and finally the original subcell structure. Despite a lack of superlattice peaks of any observable intensity, the data shows a slight preference for the structure described by supercell 2 in the case of both compounds. As the fits to the original data were unsatisfyingly similar, we sought to confirm these superlattice structures through the direct observation of superlattice peaks. To achieve this we collected data again with significantly longer counting times to improve the signal-to-noise ratio, in the hope of measuring weak diffraction peaks. In the case of the sulfur compound, there are clear diffraction peaks near $2\theta = 7.4$ and 7.8°, effectively ruling out superlattice (1) in favor of superlattice (2) (Fig. 3). The selenium compound was less conclusive, but careful examination of the diffraction pattern reveals superlattice peaks consistent with only superlattice (2) (Fig. 4). It is interesting to note that doubling the unit-cell volume, and thereby doubling the number of allowed Bragg peaks,

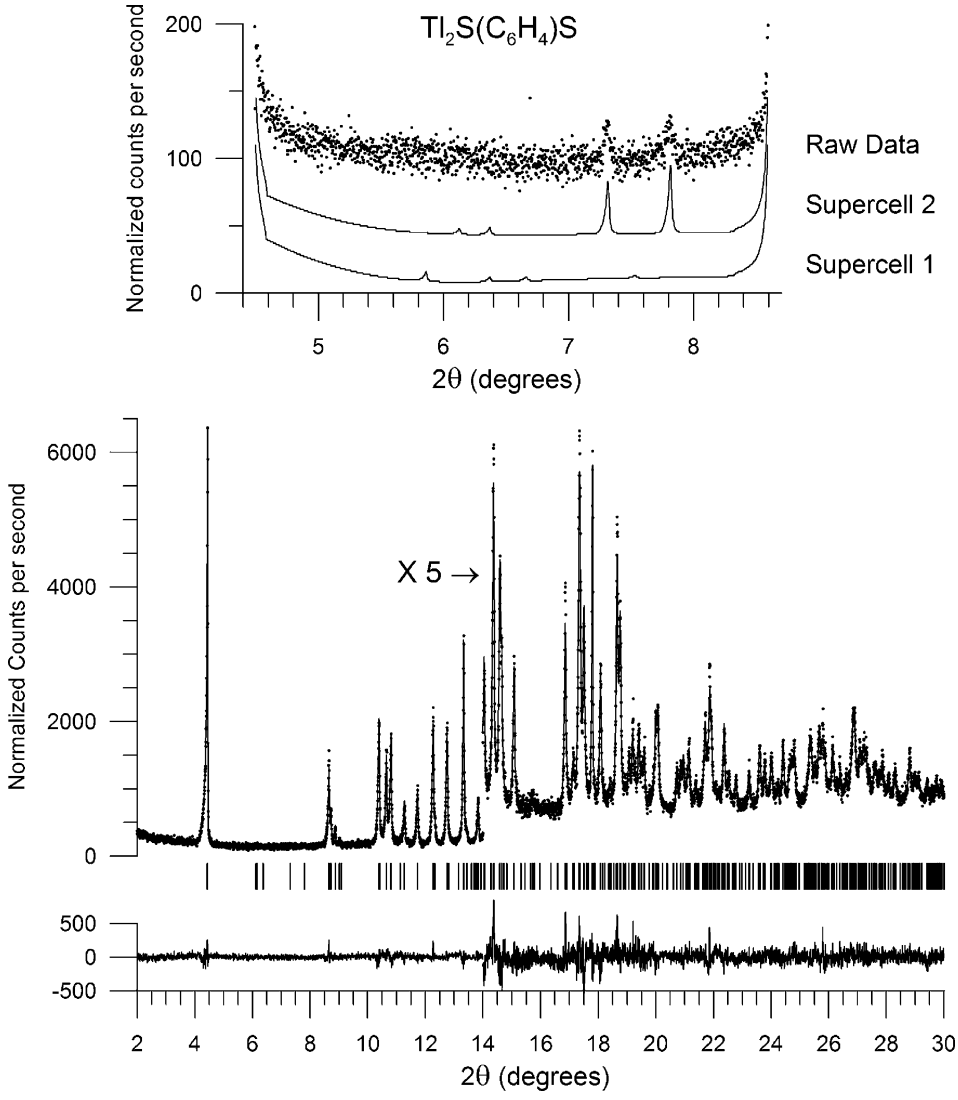

Figure 3
Rietveld plot of $Tl_2(SC_6H_4S)$. The lower panel is refinement to supercell (2) of data taken in capillary with the sample diluted with cork. Data, fit and difference curve above 14° are multiplied by a factor of five. The upper panel shows visible peaks allowed by supercell (2), from data taken in flat-plate geometry.

yields only two visible additional peaks in each powder pattern. For the purposes of comparison to the superlattice models, we have also refined the same, combined, higher statistics data against the 50–50 disordered model. Results are presented in Table 2.

For both structures, the aromatic ring was modeled as a *Z*-matrix. As it lies on an inversion center, only half of the ring was included. The S and Se atoms were included in the *Z*-matrix and constrained to lie in the plane of the ring and to extend at an angle of 120° from the next-nearest C atom. The only refinable parameters of the *Z*-matrix were the C—C bond length and the C—S or C—Se distances. The Tl atoms were located on a general position. Isotropic displacement parameters were used for both structures, with Tl atoms having their own parameter, and all other atoms sharing a single, isotropic parameter. H atoms were tethered to their respective C atoms at a distance of 1.08 Å. No hydrogen parameters were refined. All refinements were performed using *TOPAS-Academic* (Coelho, 2007).

$Tl_2(SC_6H_4S)$: The refined structure (Fig. 2*a*) has two independent SC_6H_4S molecules centered on the special positions (0,0,0) and $(\frac{1}{2},\frac{1}{2},0)$, with the planes of the rings tipped by approximately ±45° from the (superlattice) *ac* plane, *i.e.* in approximately the same orientations as the disordered model, parallel and perpendicular to the *ac* plane of the original $Z = 1$ structure. Weak peaks characteristic of superlattice (2), but not superlattice (1), are visible in Fig. 3.

$Tl_2(SeC_6H_4Se)$: The low-angle region, where the possible superlattice peaks are in a region of low, flat background, does not yield any peaks that can distinguish superlattice (1) from superlattice (2). However, there are two regions where peaks from superlattice (2) are clearly visible, shown in the insets to Fig. 4, which clearly point to superlattice (2). The structure is shown in Figs. 2(*c*) and (*d*), and the fit to the powder X-ray data is shown in Fig. 4.

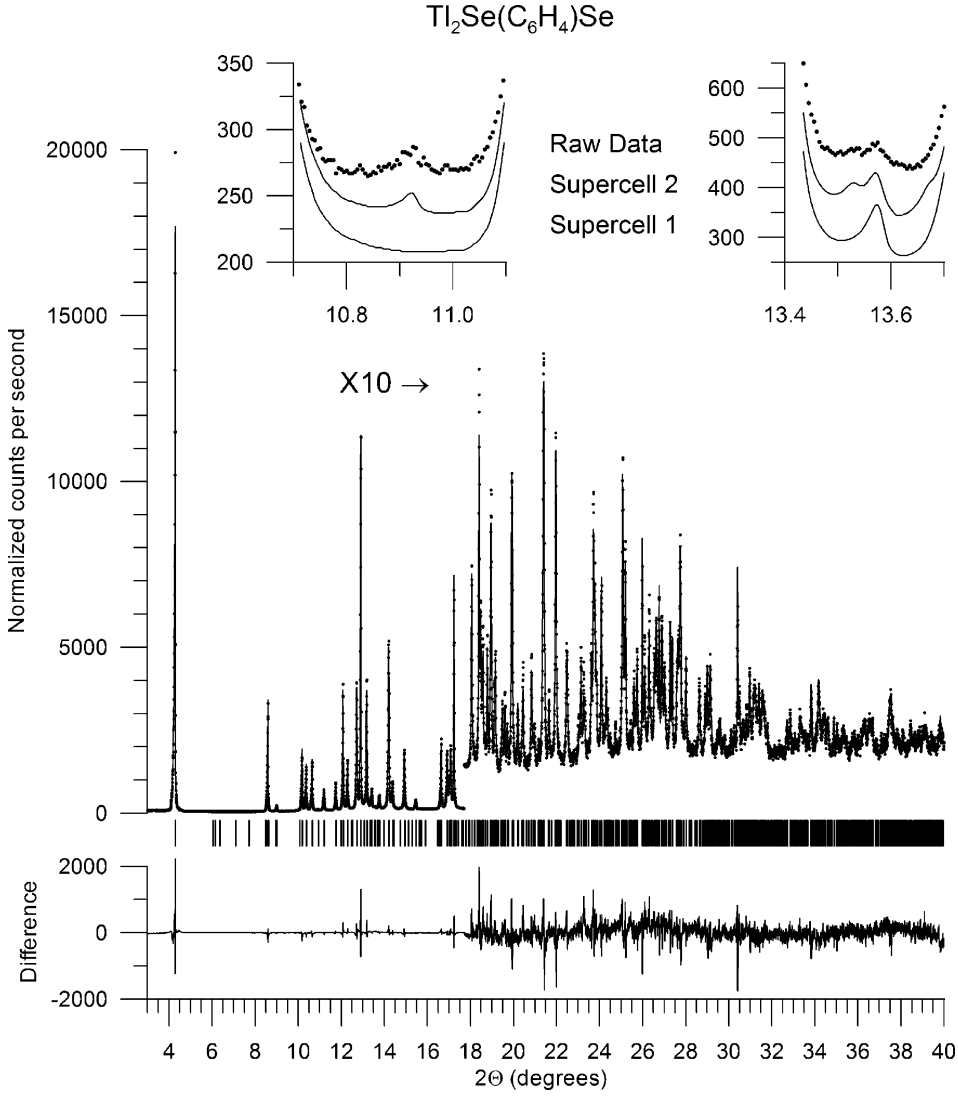

Figure 4
Rietveld plot of $Tl_2SeC_6H_4Se$. The lower panel is refinement to supercell (2) of data taken on a flat plate. Data, fit and difference curve above 17.7° are multiplied by a factor of ten. Upper panels show visible peaks allowed by supercell (2), also collected on a flat plate.

4. Structural chemistry

In both $Tl_2(SC_6H_4S)$ and $Tl_2(SeC_6H_4Se)$ the coordination sphere around each Tl atom is complex, as is commonly the case for thallium (Wiesbrock & Schmidbaur, 2003). Fig. 5 shows the coordination environment of Tl in each compound, and neighbor distances are listed in Table 3. If some particularly long Tl—S distances are considered to be bonds, each Tl is near the center of an approximate square of S or Se atoms. The shortest Tl—S distance is Tl1—S1a^{vi}, at 2.94 Å, consistent with a Tl—S bond, while the longest Tl—S interaction shown in Fig. 4 is Tl1—S1a^{iv}, at 3.92 Å, which is just slightly more than the sum of the Tl and S van der Waals radii of 3.80 Å. Typical Tl—S bond distances in the previously reported thallium thiolates discussed above range from ∼ 2.8 to 3.1 Å when the Tl is coordinated by three or fewer sulfur atoms, but can be as long as 3.410 Å (Krebs & Brömmelhaus, 1989, 1991) or 3.60 Å (Hammerschmidt *et al.*, 2005) in interactions that are still considered bonds.

The analogous Tl—Se distances range from 3.17 to 3.68 Å. In addition to those four S or Se atoms, there is an additional S or Se from the next layer in the structure (S1a^{iii}, S1^{v}, Se1a^{iii} or Se1^{v}) that is

within bonding distance to the Tl. These S or Se sit at a position such that they are apical in a square pyramid of S or Se around the Tl, but are highly distorted from an ideal square pyramid, with a minimum S—Tl—S angle around 66° (and analogous Se—Tl—Se angle around 63°). In addition to the five S or Se atoms in a distorted square pyramid, there are two separate Tl···Tl interactions at 3.49 and 3.58 Å in the sulfur compound and at 3.54 and 3.63 Å in the selenium compound. These nearby Tl atoms occupy a position near where the apex of the square pyramid would be, but, like the sulfur, they are displaced from that apical site, with a minimum S^{v}—Tl2^{i}—Tl2 angle of 50° and analogous Se1a^{iv}—Tl1—Tl1^{ii} angle of 53°. There is a second Tl1—Tl2 interaction at ∼3.9 Å in both compounds. Finally there is an open coordination site at each Tl that is consistent with a stereochemically active lone pair on Tl^{I}. The open site is opposite S1a^{iii} and Tl^{ii} that approach the apex of the square pyramid.

The $Tl^{I}\cdots Tl^{I}$ interactions present in both compounds merit further discussion. A Tl^{I} ion has a valence electron configuration of $6s^{2}5d^{10}$, and can bond with another Tl^{I} only through closed-shell interactions; such interactions are now well known for thallium (Janiak & Hoffmann, 1990; Bosch *et al.*, 1996; Childress *et al.*, 2006; Ghosh *et al.*, 1999; Wright *et al.*, 2005). Of the previously reported Tl^{I} thiolates discussed above, only $[NEt_4]_2[Tl_2(S_2C_6H_4)_2]$ has a short Tl—Tl distance [3.5116 (4) Å], indicating a closed-shell $Tl^{I}\cdots Tl^{I}$ 'thallophilic' bonding interaction. The constrained geometry of the S atoms on the SC_6H_4S ligands may affect the Tl—Tl distance in that compound, but the distance is strikingly similar to that in the present 1,4-benzenedithiolate compound.

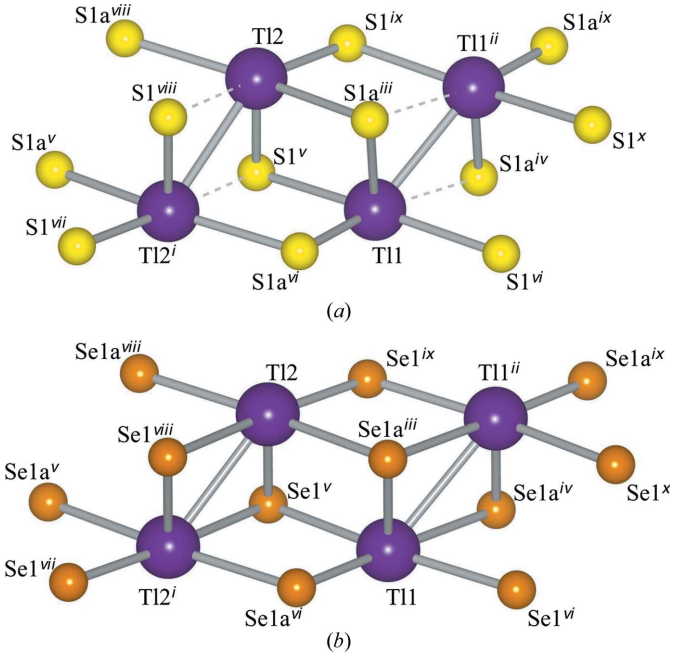

Figure 5
Coordination environment of the Tl atoms in (*a*) $Tl_2(SC_6H_4S)$ and (*b*) $Tl_2(SeC_6H_4Se)$. Atom labels correspond to those in the tables of interatomic distances.

Table 3
Selected interatomic distances (Å).

Numbers in parentheses are standard uncertainties from the least-squares Rietveld fit, and should be regarded as several times smaller than the accuracy of the determination.

$Tl_2(SC_6H_4S)$			
Tl1···Tl1^{ii}	3.488 (7)	Tl2···Tl2^{i}	3.582 (7)
Tl1···S1a^{vi}	2.938 (4)	Tl2···S1^{v}	3.075 (4)
Tl1···S1a^{iii}	3.231 (5)	Tl2···S1^{ix}	3.119 (4)
Tl1···S1^{vi}	3.232 (3)	Tl2···S1a^{viii}	3.207 (3)
Tl1···S1^{v}	3.348 (3)	Tl2···S1a^{iii}	3.448 (3)
Tl1···S1a^{iv}	3.922 (4)	Tl2···S1^{viii}	3.748 (4)
$Tl_2(SeC_6H_4Se)$			
Tl1···Tl1^{ii}	3.625 (7)	Tl2···Tl2^{i}	3.539 (6)
Tl1···Se1a^{vi}	3.166 (4)	Tl2···Se1^{ix}	3.181 (4)
Tl1···Se1^{vi}	3.239 (3)	Tl2···Se1a^{viii}	3.298 (3)
Tl1···Se1a^{iii}	3.266 (5)	Tl2···Se1^{v}	3.341 (4)
Tl1···Se1^{v}	3.463 (3)	Tl2···Se1a^{iii}	3.389 (3)
Tl1···Se1a^{iv}	3.684 (4)	Tl2···Se1^{viii}	3.679 (4)

Symmetry codes: (i) $-x, -y+1, -z+1$; (ii) $-x+1, -y+2, -z+1$; (iii) $x, y, z+1$; (iv) $-x+1, -y+2, -z$; (v) $-x, -y+1, -z$; (vi) $-x+1, -y+1, -z$; (vii) $-x, -y, -z$; (viii) $x, y, z+1$; (ix) $x, y+1, z+1$; (x) $x+1, y+1, z+1$.

In $Tl_2(SC_6H_4S)$ and $Tl_2(SeC_6H_4Se)$, the short Tl1—Tl1^{ii} distances range from 3.49 Å (sulfur compound) to 3.63 Å (selenium compound), indicative of fairly strong interactions. The longer Tl1—Tl2 interaction at 3.9 Å (in both compounds) is just slightly shorter than twice the van der Waals radius of thallium, 4.00 Å. If both types of Tl—Tl interactions are considered significant, there are zigzag chains of Tl^{I} ions in each structure.

We are extremely grateful to Professor Ton Spek for pointing out the flaw in the initial structure determination. This work was partially supported by the University of Alabama. Use of the National Synchrotron Light Source, Brookhaven National Laboratory, was supported by the US DOE, BES (DE-AC02-98CH10886).

References

Adams, R. & Ferretti, A. (1959). *J. Am. Chem. Soc.* **81**, 4939–4940.
Boer, B. de, Meng, H., Perepichka, D. F., Zheng, J., Frank, M. M., Chabal, Y. J. & Bao, Z. (2003). *Langmuir*, **19**, 4272–4284.
Bosch, B. E., Eisenhawer, M., Kersting, B., Kirschbaum, K., Krebs, B. & Giolando, D. M. (1996). *Inorg. Chem.* **35**, 6599–6605.
Childress, M. V., Millar, D., Alam, T. M., Kreisel, K. A., Yap, G. P., Zakharov, L. N., Golen, J. A., Rheingold, A. L. & Doerrer, L. H. (2006). *Inorg. Chem.* **45**, 3864–3877.
Coelho, A. A. (2003). *J. Appl. Cryst.* **36**, 86–95.
Coelho, A. A. (2007). *TOPAS-Academic*, Version 3, http://www.topas-academic.net.
Dollase, W. A. (1986). *J. Appl. Cryst.* **19**, 267–272.
Farrugia, L. J. (1997). *J. Appl. Cryst.* **30**, 565.
Ghosh, P., Rheingold, A. L. & Parkin, G. (1999). *Inorg. Chem.* **38**, 5464–5467.
Hammerschmidt, A., Brömmelhaus, A., Laege, M. & Krebs, B. (2005). *Inorg. Chim. Acta*, **358**, 4247–4252.
Janiak, C. & Hoffmann, R. (1990). *J. Am. Chem. Soc.* **112**, 5924–5946.
Krebs, B. & Brömmelhaus, A. (1989). *Angew. Chem. Int. Ed.* **28**, 1682–1683.

Krebs, B. & Brömmelhaus, A. (1991). *Z. Anorg. Allg. Chem.* **595**, 167–182.
Labahn, D., Pohl, E., Herbst-Irmer, R., Stalke, D., Roesky, H. W. & Sheldrick, G. M. (1991). *Chem. Ber.* **124**, 1127–1129.
Macrae, C. F., Edgington, P. R., McCabe, P., Pidcock, E., Shields, G. P., Taylor, R., Towler, M. & van de Streek, J. (2006). *J. Appl. Cryst.* **39**, 453–457.
March, A. (1932). *Z. Kristallogr.* **81**, 285–297.
Testaferri, L., Tiecco, M., Tingoli, M., Chianelli, D. & Montanucci, M. (1983). *Synthesis*, pp. 751–755.
Turner, D. L., Stone, K. H., Stephens, P. W. & Vaid, T. P. (2010). *Dalton Trans.* **39**, 5070–5073.
Turner, D. L., Vaid, T. P., Stephens, P. W., Stone, K. H., DiPasquale, A. G. & Rheingold, A. L. (2008). *J. Am. Chem. Soc.* **130**, 14–15.
Westrip, S. P. (2010). *J. Appl. Cryst.* **43**, 920–925.
Wiesbrock, F. & Schmidbaur, H. (2003). *J. Am. Chem. Soc.* **125**, 3622–3630.
Wright, R. J., Phillips, A. D., Hino, S. & Power, P. P. (2005). *J. Am. Chem. Soc.* **127**, 4794–4799.